V. 119, NO. 4
JULY 2022

ACI STRUCTURAL JOURNAL

A JOURNAL OF THE AMERICAN CONCRETE INSTITUTE

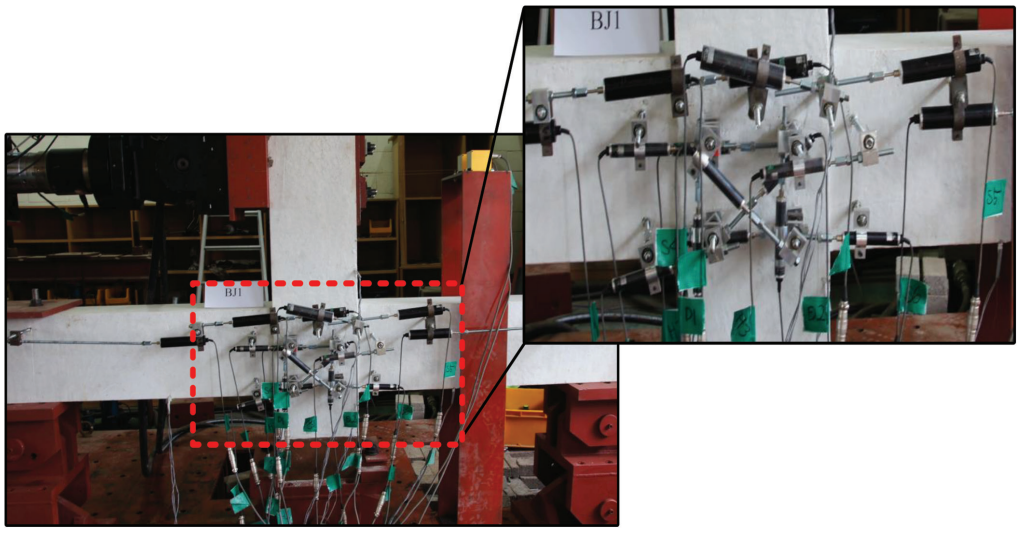

American Concrete Institute

CONTENTS

ACI Structural Journal

JULY 2022, V. 119, No. 4

A JOURNAL OF THE AMERICAN CONCRETE INSTITUTE
AN INTERNATIONAL TECHNICAL SOCIETY

Contents continued on next page

Discussion is welcomed for all materials published in this issue and will appear ten months from this journal's date if the discussion is received within four months of the paper's print publication. Discussion of material received after specified dates will be considered individually for publication or private response. ACI Standards published in ACI Journals for public comment have discussion due dates printed with the Standard.

The *ACI Structural Journal* (ISSN 0889-3241) is published bimonthly by the American Concrete Institute. Publication office: 38800 Country Club Drive, Farmington Hills, MI 48331. Periodicals postage paid at Farmington, MI, and at additional mailing offices. Subscription rates: $189 per year, payable in advance. POSTMASTER: Send address changes to: *ACI Structural Journal*, 38800 Country Club Drive, Farmington Hills, MI 48331.

Canadian GST: R 1226213149.

Direct correspondence to 38800 Country Club Drive, Farmington Hills, MI 48331. Telephone: +1.248.848.3700. Facsimile (FAX): +1.248.848.3701. **Website: http://www.concrete.org.**

CONTENTS

ACI CONCRETE CONVENTION: FUTURE DATES

2022—October 23-27, Hyatt Regency Dallas, Dallas, TX
2023—April 2-6, Hilton San Francisco Union Square, San Francisco, CA
2023—Oct. 29-Nov. 2, Boston Convention Center & Westin Boston Waterfront, Boston, MA
2024—March 24-28, Hyatt Regency New Orleans, New Orleans, LA

For additional information, contact:
Event Services, ACI
38800 Country Club Drive
Farmington Hills, MI 48331
Telephone: +1.248.848.3795
e-mail: conventions@concrete.org

ON COVER: 119-S76, p. 55, Fig. 3—Deflection and strain measurement system details.

Contributions to *ACI Structural Journal*

The *ACI Structural Journal* is an open forum on concrete technology and papers related to this field are always welcome. All material submitted for possible publication must meet the requirements of the "American Concrete Institute Publication Policy" and "Author Guidelines and Submission Procedures." Prospective authors should request a copy of the Policy and Guidelines from ACI or visit ACI's website at **www.concrete.org** prior to submitting contributions.

Papers reporting research must include a statement indicating the significance of the research.

The Institute reserves the right to return, without review, contributions not meeting the requirements of the Publication Policy.

All materials conforming to the Policy requirements will be reviewed for editorial quality and technical content, and every effort will be made to put all acceptable papers into the information channel. However, potentially good papers may be returned to authors when it is not possible to publish them in a reasonable time.

Discussion

All technical material appearing in the *ACI Structural Journal* may be discussed. If the deadline indicated on the contents page is observed, discussion can appear in the designated issue. Discussion should be complete and ready for publication, including finished, reproducible illustrations. Discussion must be confined to the scope of the paper and meet the ACI Publication Policy.

Follow the style of the current issue. Be brief—1800 words of double spaced, typewritten copy, including illustrations and tables, is maximum. Count illustrations and tables as 300 words each and submit them on individual sheets. As an approximation, 1 page of text is about 300 words. Submit one original typescript on 8-1/2 x 11 plain white paper, use 1 in. margins, and include two good quality copies of the entire discussion. References should be complete. Do not repeat references cited in original paper; cite them by original number. Closures responding to a single discussion should not exceed 1800-word equivalents in length, and to multiple discussions, approximately one half of the combined lengths of all discussions. Closures are published together with the discussions.

Discuss the paper, not some new or outside work on the same subject. Use references wherever possible instead of repeating available information.

Discussion offered for publication should offer some benefit to the general reader. Discussion which does not meet this requirement will be returned or referred to the author for private reply.

Send manuscripts to:
http://mc.manuscriptcentral.com/aci

Send discussions to:
Journals.Manuscripts@concrete.org

ACI STRUCTURAL JOURNAL TECHNICAL PAPER

Title No. 119-S81

Experimental and Numerical Analysis of Steel and Fiber-Reinforced Polymer Concrete Beams under Transverse Load

by Ahmed H. Ali, Ahmed Gouda, Hamdy M. Mohamed, and Hala Mamdouh Esmael

*Several approaches were used to explore the characteristics of reinforced concrete (RC) structural elements. Experimental work in the lab was extensively used as a means to examine the structural response and influence of different parameters under shear loads. Also, using numerical analysis to look into these components has been proven effective. This paper focuses on the shear conduct and response of circular beams reinforced with steel bars using the finite element (FE) model by considering the effect of reinforcement type and ratio, shear span-depth ratio (*a/d*), and member's size. The FE model results were confirmed with the experimental outcomes of full-scale circular RC specimens tested earlier by scientists. The outcomes from the numerical study displayed that the proposed finite element replica was capable of simulating the characteristics of the beams, tested experimentally in the lab, with credible accuracy. From the FE model, it was found that the concrete shear contribution is best described as a formula that is inversely proportional to the member's depth and directly proportional to the square root of axial stiffness of the reinforcement.*

Keywords: circular beams; finite element (FE); flexural reinforcement ratio; ratio; shear span-depth ratio (*a*/*d*); shear strength; size effect; steel.

INTRODUCTION

Circular reinforced concrete (RC) members exist in many types of structures. Many of these members usually experience severe transversal/shear loads generated from earthquakes and/or wind stresses. As a consequence, a significant amount of shear load is applied to the member's cross section (Ali et al. 2020). Realizing and grasping the behavior of the RC members during loading is paramount to construct a completely safe and efficacious structure. In the last decade, the shear strength of fiber-reinforced polymer (FRP) RC members with rectangular cross sections received considerable attention. The experimental work focused mainly on beams without web reinforcement, but limited research has addressed beams with circular cross section. Yet, no finite element model or numerical equations have investigated circular concrete members reinforced with steel or FRP reinforcement under shear loads. In general, shear design provisions can be applied to circular members by using an equivalent rectangular cross section. The accuracy of such an approach should, however, be assessed because a circular section may not contribute to shear strength in the same way as a rectangular section. Circular members usually have longitudinal reinforcement uniformly distributed around the section's perimeter. This reinforcement reduces crack propagation above the neutral axis and limits crack width, which, in turn, increases the contributions of aggregate interlock. Moreover, these bars add to the dowel mechanism in resisting the relative transverse displacement between two segments of a beam separated by a crack bridged by the reinforcement. Thus, longitudinal bars distributed through the depth might significantly affect the shear strength of circular concrete members.

Many analysis techniques have been applied to investigate the behavior and characteristics of the RC members (Mukhopadhyay et al. 2018). The results of the experimental testing were extensively used as a means to examine the structural members. Nevertheless, it's quite time-consuming and resources to build the RC members can be very expensive to use. Therefore, the finite element (FE) model is used to investigate the behavior and response of these structural elements under axial, flexural, and shear loads (De Domenico et al. 2014). Regrettably, early endeavors to achieve this were extremely time-consuming and infeasible with the preexisting software and hardware. Due to advances in knowledge and capabilities of computer software and hardware, the use of numerical analysis increased a great degree to analyze concrete structural components (Magliulo et al. 2014; Lee et al. 2020). Recently, FE programs improved and became a more efficient and precise mechanism for investigating complex structural members, therefore providing an adequate and flexible technique for covering the problems correlated with the analyses of RC members. Those problems included concrete cracking, creep, nonlinearity, and shrinkage; steel bars' rupture, and adherence between the steel bars and concrete. Nevertheless, the capabilities of FE software have to be endorsed against the outcomes of the experimental work. The results obtained by the FE method are not beneficial unless the essential procedures are considered to determine what is occurring in the FE model built with the computer program. Effective and improved analyses can be obtained by grasping the FE packages, which will lead to completely realizing the behavior of structural elements and their charactersitics within the whole structure (Halahla 2018).

The goal of this paper is to study the effect of different parameters on the behavior of circular RC beams using a specialized FE package (Atena 3D). As a first step and to achieve that goal, five RC beams were constructed and tested to failure in the lab; afterword, the exactness of the FE specimens were verified with the experimental data obtained from the RC beams (Ali et al. 2020). The verification

ACI Structural Journal, V. 119, No. 4, July 2022.

MS No. S-2021-112.R3, doi: 10.14359/51734651, received November 10, 2021, and reviewed under Institute publication policies.

Table 1—Summary of experimental results

Specimen ID	Reinforcing material	f_c', MPa	Reinforcement ratio, %	Failure load, kN	Ultimate shear load V_{exp}, kN	Strain, με		Deflection, mm
						Bars	Concrete	
						ε_u	ε_{cu}	Δ_{mid}
BS1.5	Steel	38	1.5	627	313	7098	2611	10.5
BC1.5	CFRP	36	1.5	501	251	3901	1784	12.0
BG1.5	GFRP	38	1.5	457	229	4340	2000	15.1
BG2.5	GFRP	38	2.5	489	245	3325	1752	11.6
BG3.5	GFRP	38	3.5	603	301	3802	1644	10.7

Note: Reinforcement ratio is A_s/bd; V_{exp} is failure load/2.

Table 2—Properties of reinforcing bars

Steel bars				
Bar diameter, mm		Yield strength, MPa		Modulus of elasticity, GPa
20.0		460		200
Bar diameter, $Ø_f$* (mm)	Nominal cross-sectional area, A_f (mm^2)	Guaranteed tensile strength, f_{fu}† (MPa)	Modulus of elasticity, E_f (GPa)	Tensile strain, ε_{fu} (με)
GFRP bars				
20 (No. 6)	285	1105	63.7 ± 2.5	17,300
CFRP bars				
15 (No. 5)	198	1679	141 ± 2.5	12,000

*Numbers in parentheses are manufacturer's bar designations.

†Guaranteed tensile strength: average value is 3× standard deviation (ACI 440.1R-15).

process included tracing the deformability of the specimens and strains in the concrete at the midspan, and the reinforcing bars at different locations in addition to the load-carrying capacity.

RESEARCH SIGNIFICANCE

Large research studies were conducted on shear behavior of rectangular RC elements with steel reinforcement. Very limited studies, however, were conducted and assessed the shear behavior of circular concrete elements reinforced with steel bars. More emphasis should be done regarding the structural applications of "circular beams" (axial load very small or zero) because these elements exhibit a completely different behavior than "circular columns"(big axial load). An example of circular beams is piles in ship docks with a lateral load and very small axial load.

This paper presents an experimental and FE model to assess the structural behavior and strength of circular concrete elements reinforced with steel and FRP bars. The outcome mentioned in this paper might be useful for designers using reinforced bars in concrete structures and for the development of codes and standards.

EXPERIMENTAL STUDY

To construct the beams, ready mixed concrete with normalweight concrete was used and the design strength for the specimens was 36 MPa. At the day of testing, for each beam, five 100 x 200 mm concrete cylinders were tested to capture the true compressive strength (Table 1). The flexural reinforcing bars' mechanical characteristics are seen in Table 2.

Five concrete specimens were tested to shear failure. The specimens were examined under four-point bending as seen in Fig. 1 and had a length of 3.0 m and diameter of 0.5 m. A servo-controlled, hydraulic MTS actuator with 1000 kN attached to a spreader steel beam was used to apply the loads to the circular beams, using a rate of 0.6 mm/min (displacement-controlled). The outcomes of the specimens experimentally tested can be seen in Table 1, which include the captured deformability, reinforcing bars' strain, and concrete's strain at the midspan, in addition to the load-carrying capacity and failure shear load.

NUMERICAL ANALYSIS USING FINITE ELEMENT METHOD

Mathematical numerical analyses using the FE software package TENA (Cervenka et al. 2013) was conducted in this study to imitate the shear behavior of circular RC beams reinforced with steel rods. Various parameters take FE modeling into account, such as the dimensions of the beams, types of elements, properties of the used materials, mesh size and sensitivity, boundary conditions, and types and increments of the applied loads.

The experimental specimens were used to evolve a modeling mechanism and for checking of the FE analyses outcomes (Ali et al. 2020). The FE specimens were then used to examine the effect of reinforcement ratio, modulus of elasticity, shear span-depth ratio (a/d), and member size on shear strength and behavior of steel RC beams with circular cross section area.

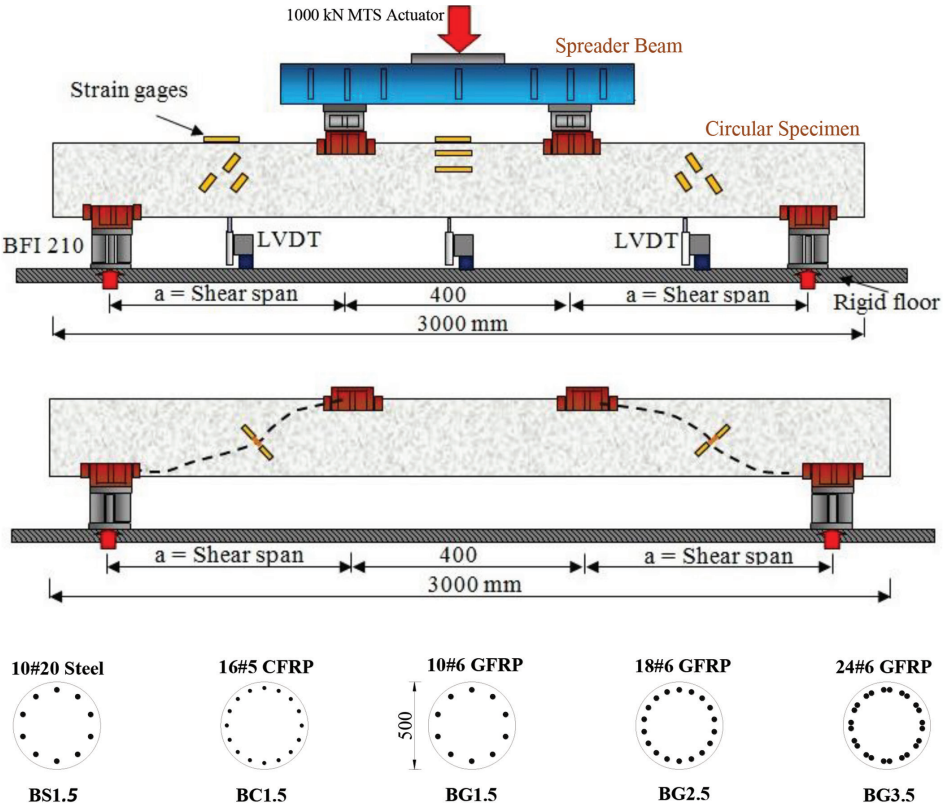

Fig. 1—Overview of specimen dimensions and test setup.

Material modeling used for steel-RC beams

Concrete—The concrete elements were modeled using rectangular and triangular brick elements. In this essay, the chosen model to build the concrete elements is known as *CC3DNonLinCementitious2*. The fracture mathematical code uses Rankine failure characteristics, whereas the nonlinear mathematical code uses the Menétrey-Willam failure surface (Cervenka et al. 2013). The mathematical codes employed by the program take into account the nonlinear behavior of the concrete material in addition to the crushing and cracking features in the three orthogonal directions.

Figure 2(a) demonstrates the unidirectional nonlinear stress-strain relationship. Before and up to the ultimate stress, the relation is established on the equation employed by the CEB-FIP Model Code (Cervenka et al. 2013). This formula can be applied to all concrete types including normal- and high-strength concrete. Subsequent to cracking or reaching the tensile capacity of the concrete elements, the formula demonstrated by the software in tension is expressed by a mathematical exponent of the crack opening equation that was found by Hordijk (1991). Furthermore, the inclination—the positive tangent modulus of the stress-strain relation at any particular point—is used to calculate the concrete's stiffness for the trial-and-error iterations employed by the software.

Reinforcing bars—Link elements (*CCIsoTruss*) were considered with three transition degrees of freedom in the three orthogonal directions at each element's node to model the flexural reinforcement. Different stress-strain relationships were used for the reinforcing rods. Glass fiber-reinforced polymer (GFRP) and carbon fiber-reinforced polymer (CFRP) reinforcement were defined as linear elastic stress-strain using the mechanistic characteristics presented in Table 2. For the steel bars, the linear stress-strain relationship, with slope equal to the modulus of elasticity (200 GPa) of the bars, was modeled up to the yielding strength of the bars (460 MPa), then a constant plateau was employed up to failure. The stress-strain relationship for the steel reinforcement is depicated in Fig. 2(b).

Characterization of steel or FRP concrete interface—The interface between the concrete elements and the reinforcing bars can have considerable impact on the outcomes of the FE specimens. Therefore, even if the experimental data has not shown any sign of bond slippage, the interface between the concrete elements and the link elements were not modeled to have a perfect contact.

Two interface relationships were defined: one for the relation between the FRP link elements and the concrete material, and the other for the steel truss elements and concrete elements as depicated in Fig. 2(c). The data for the stress-strain relation for the FRP link elements was experimentally extracted from tests performed by Ali et al. (2016).

On the other hand, the stress-strain relation for the steel rods followed the data given by CEB-FIP Model Code (Cervenka et al. 2013). The utilized relation presumed for the nonconfined concrete material, which can be described as a sloping or leading upward parabolic curve followed by linear downward stress-strain relation, then a horizontal constant relationship where the slippage increased endlessly with steady stresses (Fig. 2(c)).

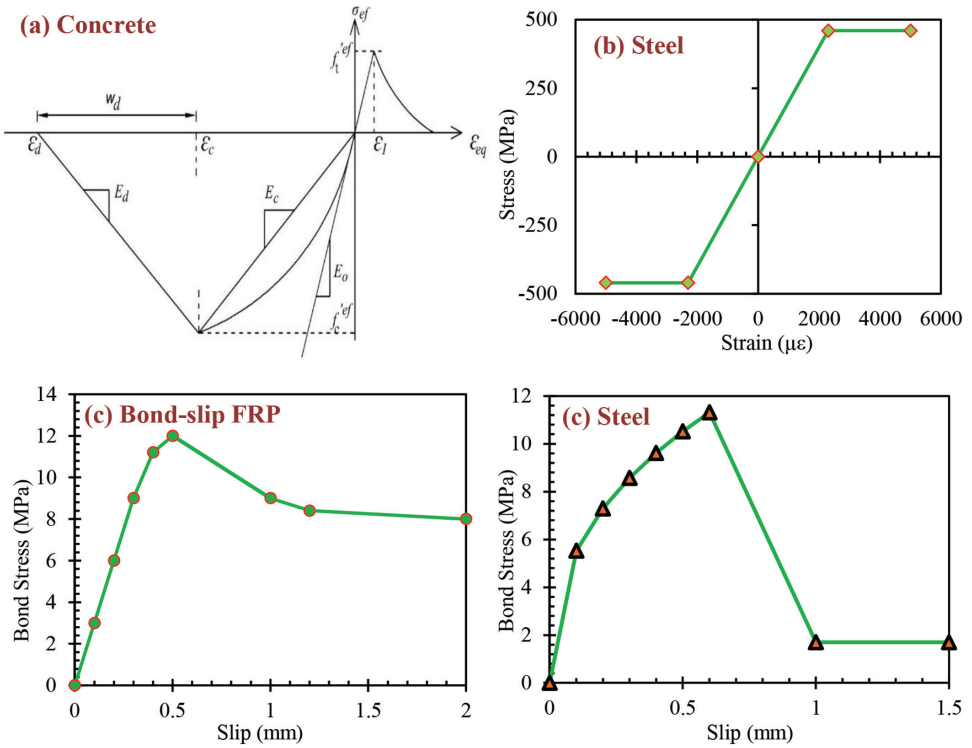

Fig. 2—Stress-strain relation: (a) uniaxial stress-strain law for concrete; (b) steel reinforcement; and (c) bond-slip relationship.

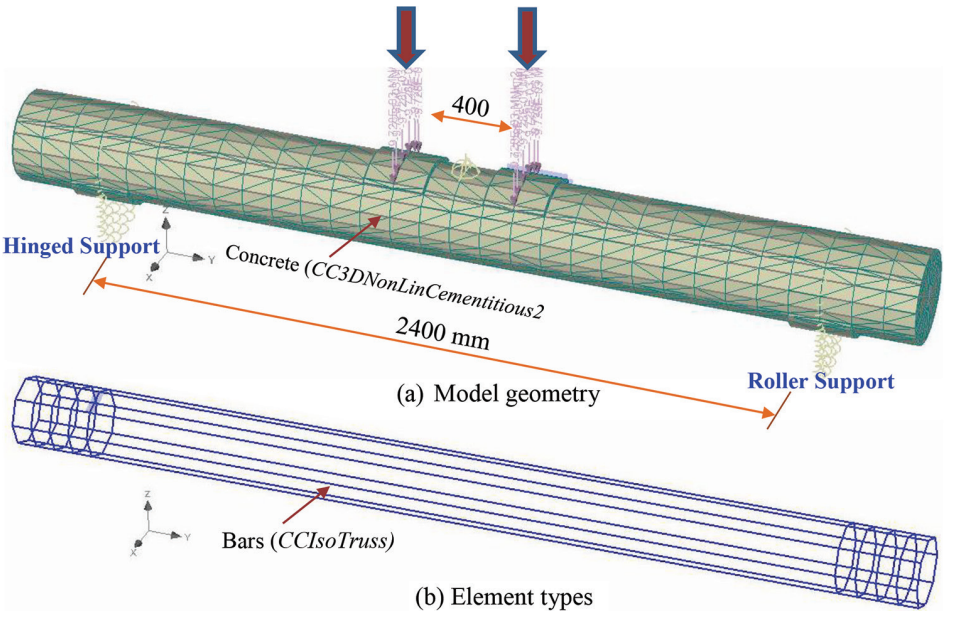

Fig. 3—Model geometry of RC beams.

FE modeling

Figure 3 depicts the geometry of the modeled beams: full actual dimensions were used and curved steel sheets were constructed at the support and load locations to imitate the shapes of the beams. The major aim for these curved steel sheets was to act as means to transfer the applied loads to the different elements of the simulated beams. A tetra element (*CCIsoTetra*) was used to build these steel sheets, with 200 GPa modulus for the elasticity and 0.3 Poisson's ratio. At the center line of each supporting sheet, the movements were constrained in the in-plan directions (x and y), which allowed the beams to rotate freely at the supports as seen in Fig. 3. The acting shear load was applied through the full surface of the two loading sheets as seen in the figure to copy the actual loading conditions from the work that was done experimentally.

Generally, selecting the right mesh size and density is a major procedure to construct any FE model, as the mesh size should be selected to give the least acceptable error. In the existing study, 0.1 m mesh size in any direction was found sufficient to get similar and close results to the experimental ones. Reducing the mesh size beyond that did not produce any additional noticeable improvement.

RESULTS AND DISCUSSION

Experimental analysis

All the circular beams tested experimentally failed in diagonal tension failure mode. The shear capacity of the circular

RC beams was found to be directly prorated to the axial rigidity of the flexural reinforcing rods. The observed post-cracking flexural stiffness of the circular FRP-RC beams to that of the steel-RC beams was close to the proportion of the axial rigidity of the FRP reinforcing rods to that of the steel ones. These results are in excellent consent with the outcomes found by many researchers, such as El-Sayed et al (2006) and Tureyen and Frosch (2002). Increasing the longitudinal flexural reinforcement ratio by approximately 68% and 129% (from 1.45% to 2.4% and from 1.45% to 3.35%) increased the failure capacity by 6.99% and 31.8%, respectively.

The prototype with the lowest axial rigidity experienced less noticeable diagonal shear cracks and had a more brittle failure mode. On the other hand, the prototype with the highest reinforcement ratio experienced totally different behavior, where the failure surface was more ductile and had deep and long diagonal shear cracks. The captured longitudinal strain in the FRP rods in all of the prototypes did not exceed 50% of the rod's ultimate tensile capacity. No bond-slippage problems were noticed in any of the beams. Four thousand three-hundred forty microstrains was the maximum measured strain in the FRP rods. Generally, the recorded strains in the FRP bars were less than the rupture strain.

On the other side and as expected, with the steel-RC prototypes, the results showed that the steel rods reached their yielding capacity at 60% of the failure shear load.

NUMERICAL RESULTS

The dimensions and material properties of the steel-prototype BS1.5 were used to build the current article. The studied variables are: 1) flexural longitudinal reinforcement ratios (starting from 0.5% up to 3.5%, with 0.5% increase) with 300 mm constant beams' diameter; 2) reinforcing bars' modulus of elasticity, steel, carbon-FRP, and glass-FRP bars with 1.5% reinforcement ratio; 3) a symmetric two-point load with a/d between 1.0 and 5.5 with a constant reinforcement ratio (1.5%); 4) a nonsymmetric one-point load with a/d extending from 1.0 to 5.5 and with the same reinforcement ratio (1.5%); and 5) size effect with different beams' diameter ranging from 300 to 500 mm and 1.5% reinforcement ratio. For every variable, a comparison was carried out for the measured deflection at the midspan, tensile strain in the reinforcing bars, compressive strain in the concrete at the midspan, crack pattern, and shear strength. Each beam's designation is composed of five symbols: the first is a symbol exemplifying the material used for the longitudinal flexure reinforcement rods ("S" represents the steel bars, whereas "G" stands for the sand-coated GFRP rods and "C" represents the sand-coated CFRP rods). The second is a digit to demonstrate the flexure longitudinal reinforcement ratio (0.5, 1.0, 1.5, and so on). The third is a number to symbolize the beam's diameter (300 mm, 400 mm, and 500 mm). The fourth is a number that stands for the span-depth ratio a/d, (1.0, 2.5, 4.0, and so on). The fifth indicates the loading conditions ("N" for just one-point load, and "Y" for two symmetrical point loads). For comparison purpose, the beams were divided into five series as shown in Table 3.

Flexure reinforcement ratio (Series I)

According to the available literature (ACI 440.1R-15), for simply supported RC members, shear stresses can be passed on by one or more of the subsequent five techniques: 1) stresses in the compressive uncracked concrete zone; 2) the interlock between aggregate's particles; 3) flexure longitudinal reinforcing rods' dowel action; 4) arch or thrust behavior (action); and 5) tensile residual stresses. Increasing the longitudinal reinforcement ratio will have a distinguished impact on enhancing the load-carrying capacity through most of these techniques. The cracks' scheme, at the failure's stage, for several FEM models is shown in Fig. 4(a). Increasing the reinforcement ratio produced higher numbers of cracks but with smaller crack spacing; this can be related primarily to the reduced bar spacing and the distribution of stresses on extra bars. Furthermore, some researchers (Gouda and El-Salakawy 2015) reported that cracks' distribution and width are directly correlated to the distance between the reinforcing bars, subsequently increasing the reinforcement ratio by increasing the bars' diameter and not the numbers of bars might not have the same effect on the crack pattern observed in the current article.

Figure 5 manifests the deformabilty at the midspan on the horizontal axis and the applied load on the vertical axis. Equivalent to the experimental findings, the attitude of the FEM specimens can be best explained as two lines with a uniform transformation between them. The increase in the deformability was approximately linear up to the formation of the initial flexural crack. The attitude of the specimens at that time illustrates the stiffness of the whole cross section of the flexural uncracked models. Once the cracks were noticed where the tensile capacity of the concrete was overran by the strength of the applied shear load, the specimens in terms of load deformability started to behave in a nonlinear relationship. That attitude represents the uncracked flexural stiffness of the models, which was constantly decreasing as the applied-load increased; however, the amount of decrease tended to be of inverse proportion against the rise of the reinforcement stiffness, $\rho_f E_f$, of the models. All the specimens, according to what is shown in the figure, followed that trend; however, the specimen with the lowest reinforcement ratio (0.5%) had two flat plateaus where the deflection increased by 10 to 38% at approximately the same load level that might indicate a sudden decrease in the stiffness, which might be due to the formation or opening of more cracks. Generally, increasing the axial stiffness from 0.5% to sevenfold of that (3.5%) enhanced the stiffness of the specimens, after cracking, which therefore reduced the deformability by approximately 83% at the same load level, and at failure by approximately 20%.

Figure 6 shows the captured strain in the steel rods at the midspan on the horizontal axis and the load-carrying capacity on the vertical axis. The captured tensile-strain was unimportant and did not go beyond 50 microstrains for all the beams. When the tensile capacity of the concrete got overran by the load-carrying capacity's tensile stress, the strains in the steel rods increased in a remarkable way. According to the test results, the reinforcing bars started to yield in all models at approximately 2300 με, which agrees with the

Table 3—Test results of all series

Specimen	Failure load, kN	Shear force, kN		Failure shear stress *Vu*, MPa		Failure strain, με		Ultimate mid-deflection, mm
		Left (Q_L)	Right (Q_R)	Left	Right	Bars	Concrete	
Series I (reinforcement ratio)								
S0.5-300-4.4-Y	103	51.5		0.715		2950	–3130	16.9
S1.0-300-4.4-Y	162	81		1.125		3560	–3120	12.1
S1.5-300-4.4-Y	228	114		1.58		5090	–3340	13.1
S2.0-300-4.4-Y	242	121		1.68		5830	–3290	13.5
S2.5-300-4.4-Y	267	133.5		1.85		8090	–3170	12.3
S3.0-300-4.4-Y	312	116		2.17		6350	–3420	13.6
S3.5-300-4.4-Y	333	166.5		2.31		8500	–3260	13.6
Series II (material type)								
S2.5-300-4.4-Y	267	133.5		1.85		8090	–3170	12.3
C2.5-300-4.4-Y	206	103		1.43		3040	–2960	11.8
G2.5-300-4.4-Y	182	91		1.26		4280	–2900	14.5
Series III (*a*/*d,* symmetric)								
S1.5-300-1.0-Y	821	410.5		5.7		1290	–2020	13.5
S1.5-300-2.5-Y	316	158		2.19		1580	–1790	10.7
S1.5-300-4.0-Y	245	122.5		1.7		5450	–3360	13.9
S1.5-300-5.5-Y	197	98.5		1.37		4530	–3590	12.2
Series IV (*a*/*d*, nonsymmetric)								
S1.5-300-1.0-N	468	410	58	5.7	0.8	2080	–890	6.11
S1.5-300-2.5-N	195	146	49	2.03	0.68	1160	–1010	6.8
S1.5-300-4.0-N	171	107	64	1.49	0.89	8720	–2120	8.39
S1.5-300-5.5-N	197	98.5		1.37		4530	–3590	12.2
Series V (size effect)								
S1.5-300-4.4-Y	228	114		1.58		5090	–3340	13.1
S2.5-300-4.4-Y	267	133.5		1.85		8090	–3170	12.3
S3.5-300-4.4-Y	333	166.5		2.31		8500	–3260	13.6
S1.5-400-3.3-Y	396	198		1.55		3000	–1520	9.31
S2.5-400-3.3-Y	432	216		1.69		3250	–2180	8.97
S3.5-400-3.3-Y	494	247		1.93		2760	–2380	10.9
S1.5-500-2.6-Y	597	298.5		1.49		5430	–2110	13.4
S2.5-500-2.6-Y	632	316		1.58		4630	–1730	8.17
S3.5-500-2.6-Y	766	383		1.915		3800	–2650	10.8

mechanistic characteristics of the deformed steel rods as shown in Table 3. Furthermore, after cracking and before yielding, increasing the steel rod's ratio led to a considerable improvement in the strain at the same load level. The tensile strain in the specimens with steel rods ratio of 1.0, 1.5, 2.0, 2.5, 3.0, and 3.5 were reduced by 15%, 34%, 40%, 53%, 59%, and 68%, respectively, in contrast to the model with 0.5% reinforcement ratio.

For the shear strength of the specimens, increasing the reinforcement ratio by seven times enhanced the ultimate shear strength by more than the double (220%) from 0.7 to 2.3 MPa, as shown in Table 3. That significant enhancement in the ultimate strength can be related to the increase in the dowel and aggregate interlock capacities through the better allocation of the cracks and stresses in the concrete members, which is directly connected to the increase in numbers of the steel rods (Mahmoud 2015). The relationship between the axial rigidity of the beams' steel rods and the failure strength is presented in Fig. 7. In addition, an interpolation formula was generated (Eq. (1)) to find the numerical connection between the failure strength and the rigidity of the beams' longitudinal steel rods. The method of the least squares was used to come up with the formula. Corresponding to the outcomes of this equation, the failure-strength was decided to be directly proportional to the rigidity of the beams' steel rods to the power of 0.595. Furthermore, the numerical constant in the formula is 0.0122.

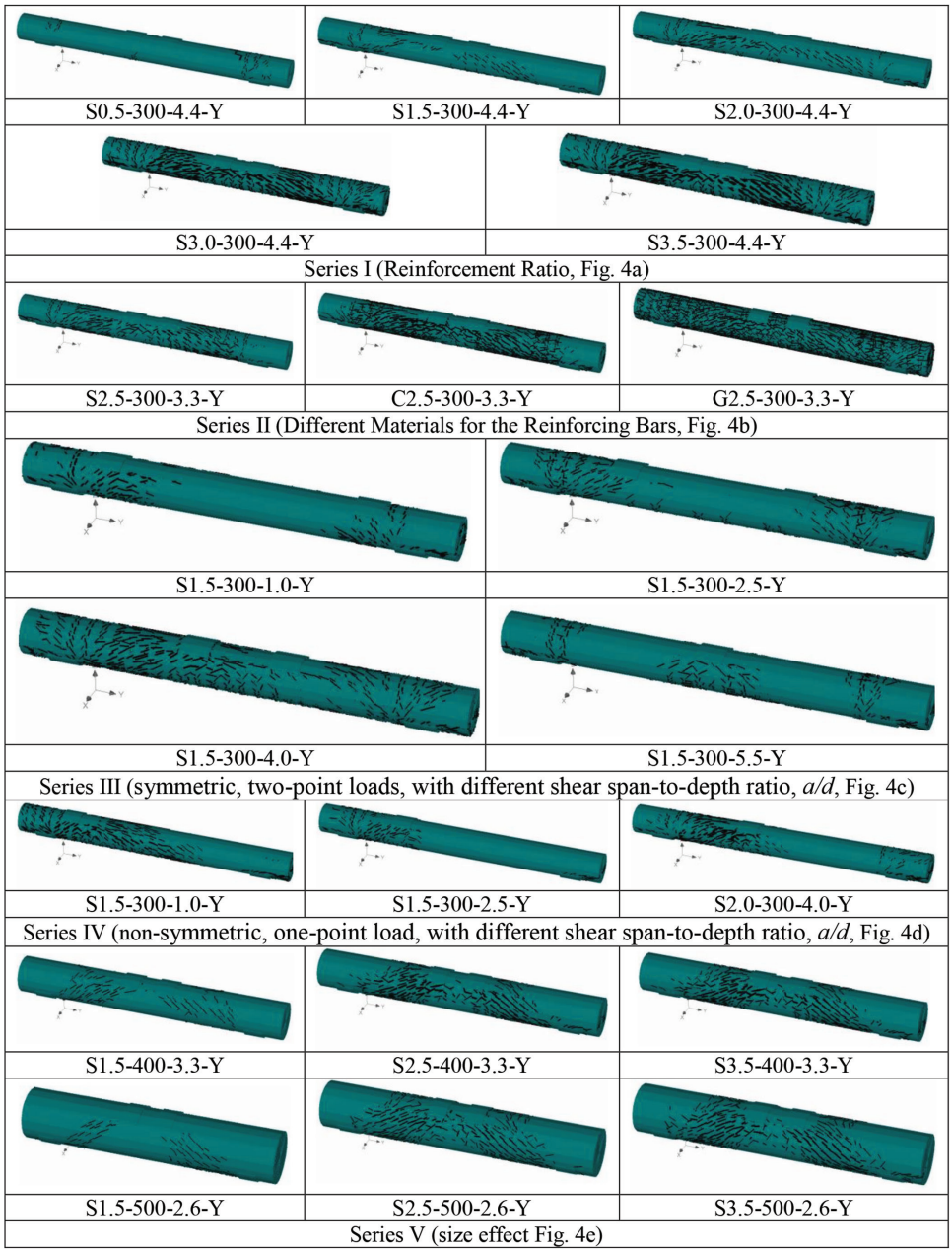

Fig. 4—Crack distribution at failure stage for all series.

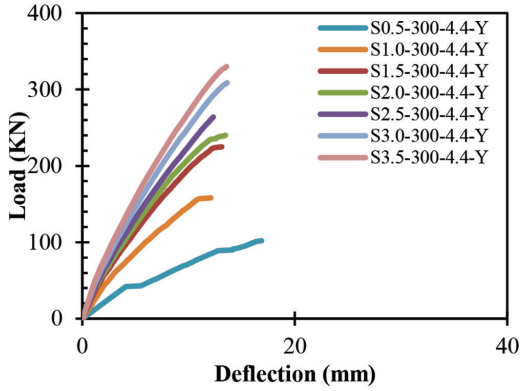

Fig. 5—Variation in load-deflection relationship with reinforcement ratio (Series I).

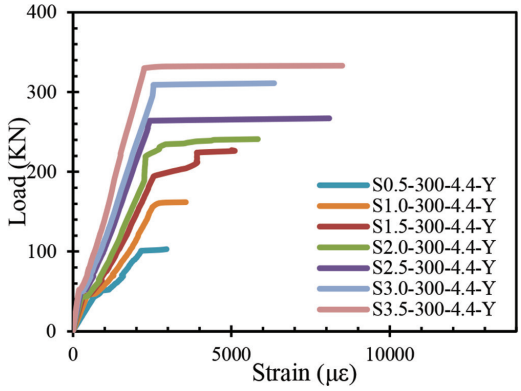

Fig. 6—Variation in load-strain relationship in reinforcing bars (Series I).

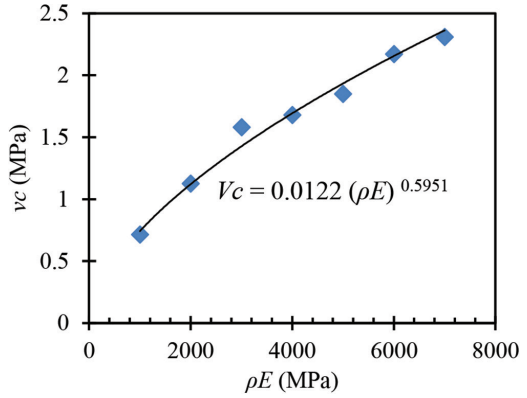

Fig. 7—Relationship between shear strength at failure and axial stiffness of reinforcement (Series I).

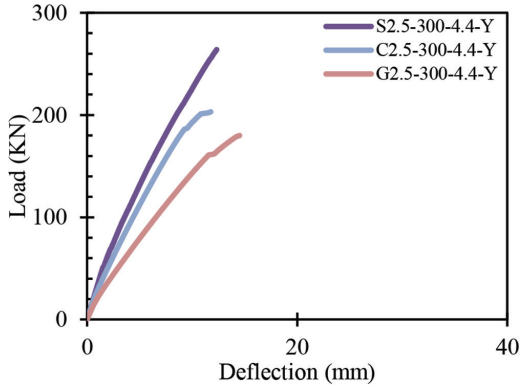

Fig. 8—Load-deflection relationship for specimens with different material types for reinforcing bars (Series II).

$$v_c = 0.0122(\rho E)^{0.595} \quad (1)$$

Material types of reinforcing bars (Series II)

The crack scheme at failure is shown in Fig. 4(b). The specimens reinforced with sand-coated bars (C2.5-300-3.3-Y and G2.5-300-3.3-Y) had smaller crack spacing in relation with the specimen reinforced with the steel mechanical deformed bars (S2.5-300-3.3-Y). That can be related, to a large extent, to the uniform allocation of the bond stress on the circumference of the sand-coated bars, in contrast to that of the steel ones where the bond is mainly through the bearing on the bar's ribs.

Figure 8 displays the vertical load versus the captured deformability at the center of the beams. The behavior of the specimens is equivalent to that explained previously in the "flexural reinforcement ratio" section. The model with sand-coated GFRP bars (G2.5-300-3.3-Y) had the least shear force and cracked stiffness. Also, due to the higher axial stiffness of S2.5-300-3.3-Y in relation to C2.5-300-3.3-Y and G2.5-300-3.3-Y, a major enhancement was noticed in the deflection. At the same carrying-shear level, increasing the modulus of elasticity of the longitudinal reinforced rods from 63.7 and 141 to 200 GPa (Table 1) reduced the deflection by approximately 60% and 30%, respectively. In addition, due to the linear and nonlinear features of the steel rods, Specimen S2.5-300-3.3-Y seemed to have more ductile behavior and a higher degree of nonlinearity. The flexural stiffness, after cracking, increased by roughly 17% and 72%

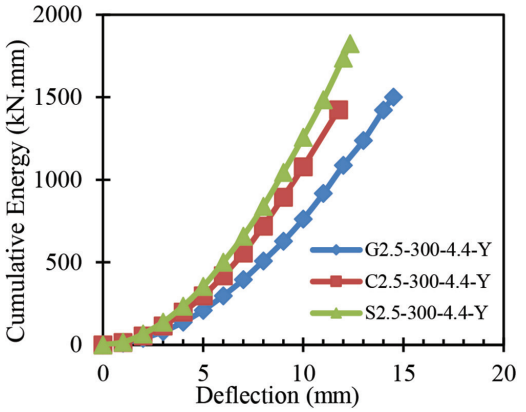

Fig. 9—Cumulative energy of specimens of Series II.

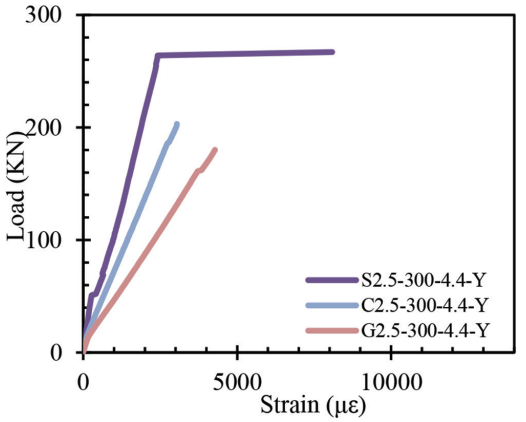

Fig. 10—Load-strain relationship in reinforcing bars for specimens with different material types for reinforcing bars (Series II).

because of the increase in the modulus of elasticity by 42% and 214%, respectively.

The accumulated energy for the specimens of the current series is shown in Fig. 9. The accumulated energy was calculated for the area under the curve shown in Fig. 8 (load-deflection relationship). Enhancing the beams' axial rigidity improved the calculated energy at the same deflection level and at failure as well. Specimen S2.5-300-3.3-Y had higher cumulative energy by 20% and 68% more than Specimens C2.5-300-3.3-Y and G2.5-300-3.3-Y, respectively, at the same deflection level, and close to 25% at failure. These findings suggest that Specimen S2.5-300-3.3-Y might have had more damage and destruction than the other two specimens at failure to release that energy. In spite of that, extra studies are still required to confirm that conclusion.

Figure 10 shows the reinforcing bars' strains captured at the center of the beams. The behavior of the specimens is comparable to that previously written in the "flexural reinforcement ratio" section. The maximum measured strain was approximately 4280 and 3040 με (Table 3) in Specimens G2.5-300-3.3-Y and C2.5-300-3.3-Y, respectively. These values of strains are approximately 25% of the maximum ultimate strain of the sand-coated GFRP and CFRP rods used in the presented project. These numbers prove that the failure of the specimens did not commence by any tear in the reinforced rods. At the post-cracking stage, the measured

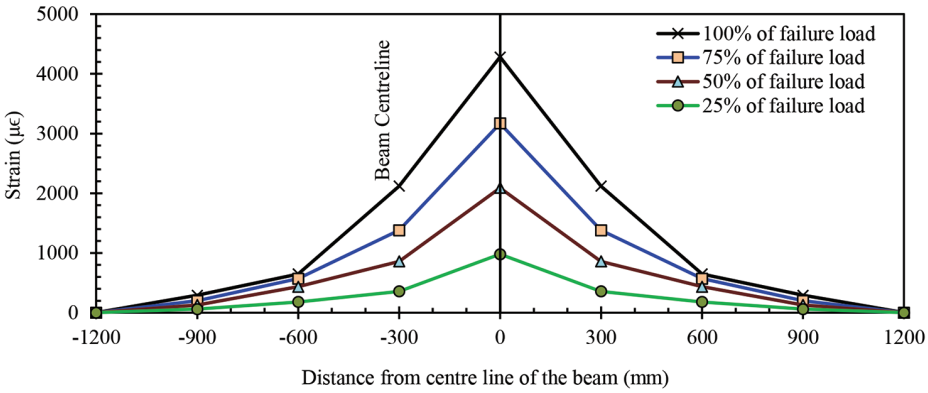

a) The GFRP specimen (G2.5-300-4.4-Y)

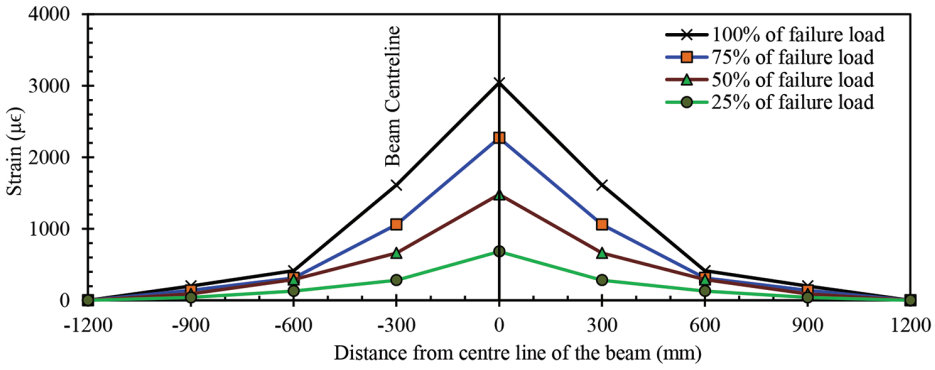

b) The CFRP specimen (C2.5-300-4.4-Y)

Fig. 11—Strain profiles in reinforcing bars at center lines of beams (Series II).

strains decreased by approximately 33% and 59% at the same load level for Specimen S2.5-300-3.3-Y with respect to Specimens C2.5-300-3.3-Y and G2.5-300-3.3-Y.

The strain profiles in the reinforcing bars at the center lines of Specimens G2.5-300-3.3-Y and C2.5-300-3.3-Y are given in Fig. 11. The figure shows that the strain is decreasing as going further from the center lines of the beams, which confirms that no bond slippage took place. This agrees and confirms the rupture strain calculated earlier and with the outcomes of other researchers (Dulude et al. 2013). On account of the relatively smaller elastic modulus of the FRP bars with respect to that of the steel ones, RC-FRP members have relatively smaller stiffness after cracking, which results in wider crack width and a smaller depth to neutral axis. Moreover, FRP rods are unidirectional materials (anisotropic) with low shear strength and stiffness in nonlongitudinal directions. This will generally result in a smaller failure load and thus low share to the RC members' shear resistance. According to that explanation and the test results presented in Table 3, Specimen S2.5-300-3.3-Y had higher shear strength than those of Specimens C2.5-300-3.3-Y and G2.5-300-3.3-Y by 29% and 53%, respectively.

Symmetric two-point loads with different shear span-depth ratio (*a*/*d*, Series III)

Four specimens with several span-depth ratios extended from 1 to 5.5 were built to evaluate the effect of that parameter. The distance between the supports was kept constant and the distance between the two-point loads was changed for every specimen to achieve the required span-depth ratio as shown in Fig. 1.

The crack distribution near the failure stage is shown in Fig. 4(c). The specimen with 5.5 span-depth ratio, S1.5-300-5.5-Y, had vertical and inclined cracks around the point of the applied load. According to Wight and MacGregor (2011), a relatively large amount of bending moment in the structure is expected with a span-depth ratio > 2.5. Subsequently, an increase in the flexural stresses is anticipated, which would lead to vertical flexural cracks. With increasing the applied load and the interaction between internal forces (shear forces and bending moment) induced in the beam, the vertical flexural cracks will form inclined ones. On the other side, Specimens S1.5-300-2.5-Y and S1.5-300-1.0-Y considered short beams, where $a/d < 2.5$. In that type of structure, arch action is the dominated attitude, whereas most of the cracks are around the supports as shown in Fig. 4(c). Meanwhile, the crack scheme associated with Specimen S1.5-300-4.0-Y is due to a combination between the effects of beam and arch actions.

Figure 12 displays the relation between the span-depth ratio and load deformability captured at the midspan of the beams. As expected, the model with span-depth ratio equal to 1.0 (S1.5-300-1.0-Y) had the highest shear strength and flexural stiffness after cracking. As the span-depth ratio decreased, a major enhancement in the shear strength and flexural stiffness can be noticed due to the increase in the

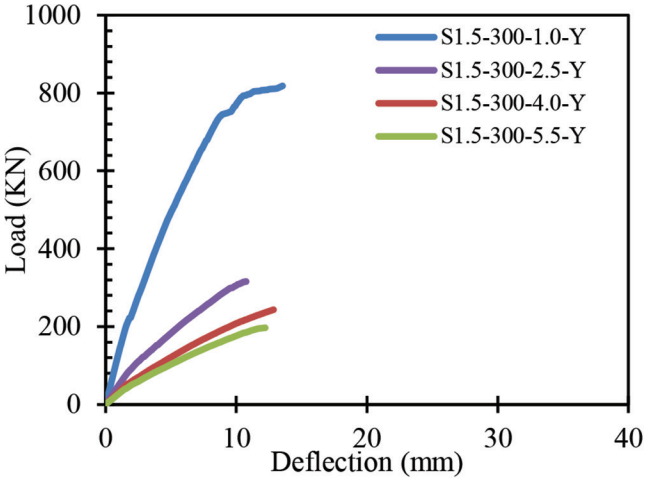

Fig. 12—Load-deflection relationship for Series III.

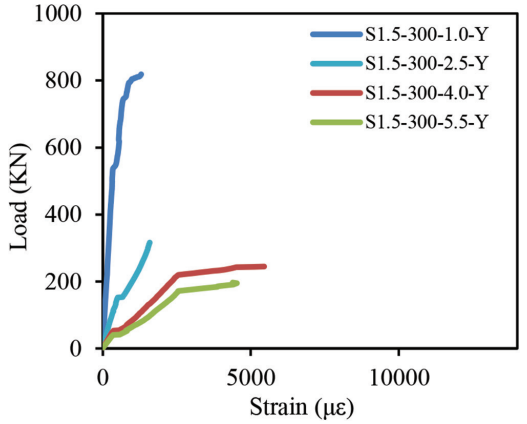

Fig. 13—Load-strain relationship for Series III.

portion of the applied load that is being transmitted directly to the supports by diagonal compression (Wight and MacGregor 2011). Specimens S1.5-300-4.0-Y, S1.5-300-2.5-Y, and S1.5-300-1.0-Y had less deformability at the same shear level by approximately 23, 50, and 87% with reference to Specimen S1.5-300-5.5-Y. Also, the same specimens experienced higher post-cracking stiffness by 40%, 107%, and 480% with respect to the model with the highest span-depth ratio (S1.5-300-5.5-Y).

Figure 13 illustrates the load-strain relationship in the reinforcing bars at the center of the beams for the investigated span-depth ratios. Models S1.5-300-5.5-Y and S1.5-300-4.0-Y started to yield at approximately 90% from the failure loads; however, Specimens S1.5-300-2.5-Y and S1.5-300-1.0-Y did not experience any yielding at all. Specimens S1.5-300-4.0-Y, S1.5-300-2.5-Y, and S1.5-300-1.0-Y had less strain at the same load level by 21%, 80%, and 96%, respectively, with consideration to Specimen S1.5-300-5.5-Y. For beams with span-depth ratios less than 2.5, behavior is predominantly governed by the impact of thrust or arch action where the reinforcing bars are acting as ties, which might explain the low strain associated with Specimens S1.5-300-2.5-Y and S1.5-300-1.0-Y. On the other hand, for span-depth ratios greater than 2.5, the behavior is dominated by the beam action, where the structure is under

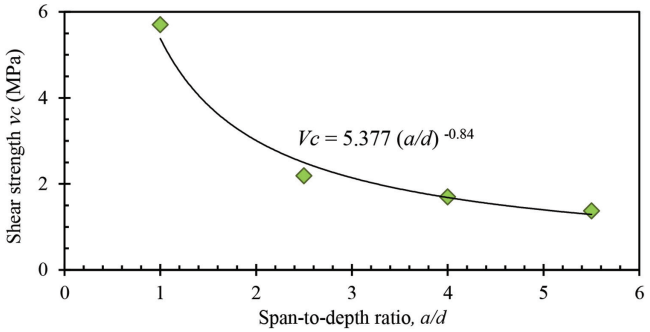

Fig. 14—Relationship between ultimate shear strength and span-depth ratio (Series III).

high bending moment; therefore, it would suffer from relatively larger strains (Kim et al. 1999).

Slenderness of the RC members, such as beams, can be measured in many ways, such as the ratio between the span and depth of the member. It's well known and established that shear strength or capacity increases whenever the ratio (a/d) decreases. For deep RC members with a/d ratio less than 2.5, this influence is more prominent, where part of the applied load is transferred through concrete compression struts that would be formed between the supports and points of the applied loads. This technique is recognized as arch or thrust action, where the shear capacity in the RC members is dominated or governed by the concrete compressive strength rather than the tensile strength. For RC members with a/d greater than 2.5, the effect of arch action on the shear capacity is insignificant and the behavior of the members is predominated or controlled by the impact of beam action (MacGregor and Bartlett 2000). The relation between the span-depth ratio and the ultimate shear load is given in Fig. 14. Specimens S1.5-300-4.0-Y, S1.5-300-2.5-Y, and S1.5-300-1.0-Y failed at higher ultimate stresses by 24%, 60%, and 316% with reference to Specimen S1.5-300-5.5-Y. The higher percentage and shear strength (Table 3) associated with Specimen S1.5-300-1.0-Y can be related to the effect of arch action associated with that specimen. These outcomes are in perfect agreement with the outcomes mentioned by numerous researchers. Kim et al. (1999) tested eight 0.3 m depth by 0.2 m width, symmetric two-point load, steel-RC beams with different span-depth ratios, ranging from 2.0 to 4.0. According to the test findings, it was reported that the ultimate stresses increased by 103% when the span to depth decreased from 4.0 to 2.0, with 1% constant reinforcement ratio. This percentage became close to 26% when the flexural reinforcement ratio increased to 2%.

Nonsymmetric one-point load with different shear span-depth ratio (a/d, Series IV)

Similar to Series III, four specimens subjected only to one-point load were constructed to study the impact of a/d. The distribution of the cracks at the ultimate stage is shown in Fig. 4(d). As seen in the figure, the cracks are concentrated at the left shorter span between the area of the applied load and left support, which is an indication of the stress's severity surrounding that region, which is definitely related to the bigger portion of the applied load that is being transferred to the near support (left) as mentioned earlier in Series

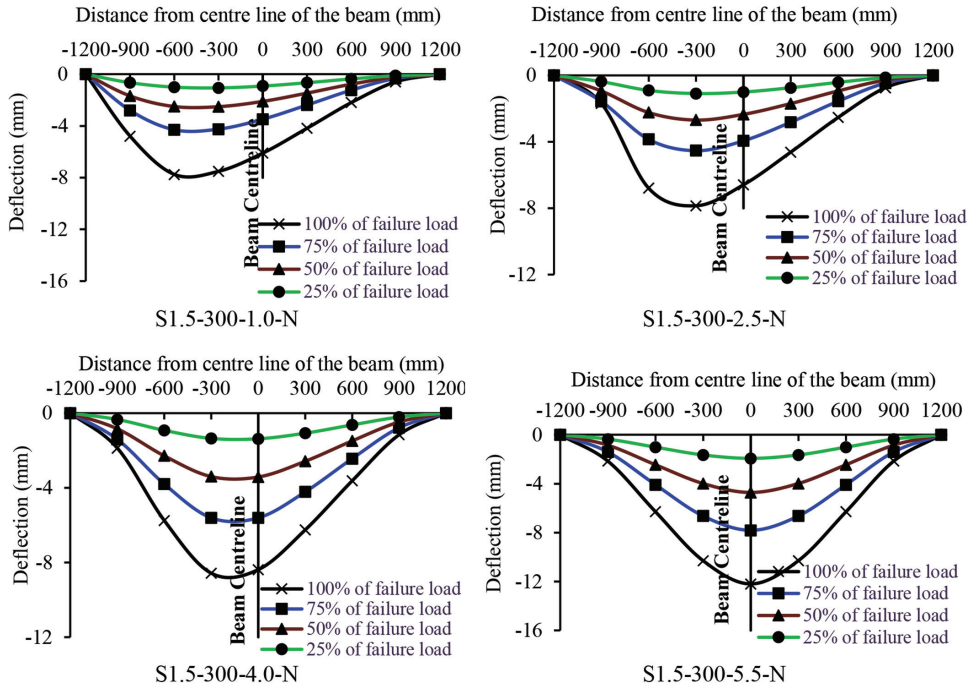

Fig. 15—Deflection profiles at centerlines of specimens for Series IV.

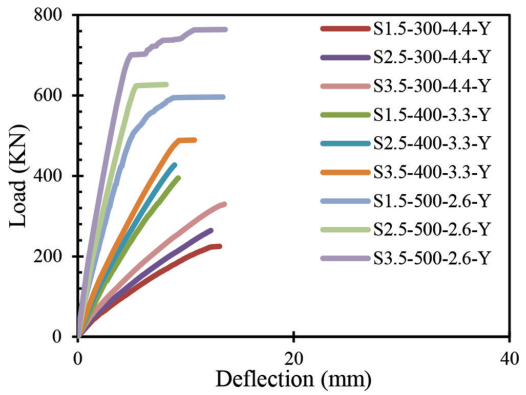

Fig. 16—Load-deflection relationship for Series V.

III. It is well known from the structural analysis principles that the maximum measured deflection for simply supported uncracked beam under static loads should be in the midspan regardless of the point(s) of application of the load(s). Figure 15 displays the deflection profiles for the tested specimens along the centerline of the beams at different loading stages. At the early loading stage, the behavior of the specimens should be in, or close to, the uncracked zone. Therefore, as can be noticed from the figure, the highest deflection at load level at approximately 25% from the failure load is at the midspan of the specimens or pretty close to it, which agrees with the principles of structural analysis for uncracked beams. Also, the location of maximum deflection seems to be moving from the center of the beam toward the left support as the point of load's application moves toward it as well. That can be illustrated by the fact that along the beam, different crack patterns and scheme would be generated. This would reduce the stiffness of the specimen in a completely random way along the beam, and that reduction in stiffness will be definitely higher close to the point of the load's application, and in turn that would induce higher deflection around that point not at or near the midspan of the beam.

As shown in Table 3, the maximum shear capacity for Specimens S1.5-300-4.0-N, S1.5-300-2.5-N, and S1.5-300-1.0-N was higher than the corresponding one for Specimen S1.5-300-5.5-N by 9%, 48%, and 316%, respectively.

Size effect (Series V)

Figure 4(e) depicts the crack allocation along the specimens. Increasing the beams' depth reduced the number of cracks at the same reinforcement ratio. This is a well-known phenomena: whenever the member's depth increased, larger crack spacings and widths were expected to develop. Some researchers even reported that double crack widths should be anticipated just for doubling the depth of the beam (Shoyia et al. 1989). A significant enhancement in the captured deflection at the mid-of-beam's span was observed as the member's diameter increased as shown in Fig. 16. This great improvement is due to the increase in flexural stiffness of the members. Increasing the depth of the beams by 33% and 66% from 300 to 400 and 500 mm reduced the measured deflection at the same shear level by approximately 58% and 83%, respectively, regardless of the reinforcement ratio. Whereas the enhancement in the stiffness after cracking was up to two and five times, respectively.

Different test results on beams show that size effect has a main influence on the shear capacity of the RC members, especially on those without web or shear reinforcement (Kani 1967; Shioya et al. 1989). Shear strength tends to decrease as the member's depth increases. As the depth of the RC members increases, greater width would develop in the diagonal shear cracks, which would minimize the capability to transfer the stress along the crack interface and the residual tensile stress. In the current study, similar behavior was generally observed for the specimens with a circular cross section. Table 3 presents the ultimate shear stresses

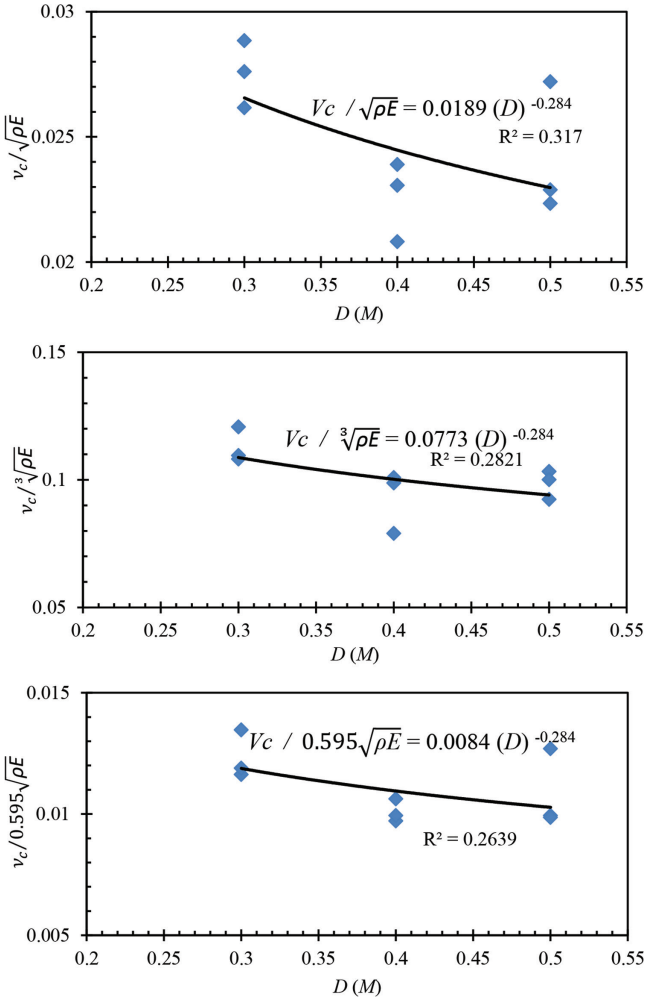

Fig. 17—Relationship between normalized ultimate strength and specimens' diameter for Series V.

resisted by the specimens; the decrease in the stresses was roughly 12% and 16% for increasing the beam's diameter from 300 mm to 400 mm and 500 mm, respectively.

Figure 17 presents an effort to try and find the correlation between the beam's diameter and the ultimate stresses sustained by the specimens; three diagrams with three equations are shown in the figure. The equations were figured out by the method of least squares, mentioned earlier. To try and find the direct relation between the ultimate strength and the member's diameter without the effect of the axial rigidity of the reinforcing rods, the ultimate strength was normalized in three different ways (square root of the reinforcement ratio, cubic root of the reinforcement ratio, and to the power that was found in Eq. (1): 0.595). However, it was found in the three diagrams that the normalized final shear strength is inversely proportional to the beam's diameter to the power of 0.28. Also, the resulted regression analysis shows that the diagram that was normalized to the square root of the axial rigidity of the reinforcement has a least coefficient of determination R^2, which indicates less scattering for the data, and that agrees with most equations in the building codes to predicate the concrete contribution to the design strength.

To help the designers and based on the analysis performed in the current article, Eq. (2) is presented to predicate the ultimate shear stresses for the concrete contribution for

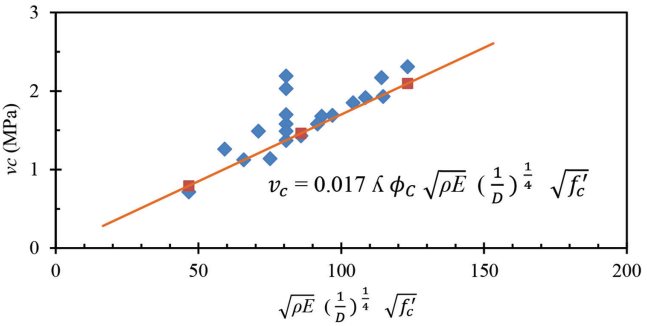

Fig. 18—Predication of ultimate strength for members with circular cross section.

members with circular cross section. As shown in Fig. 18, the presented formula is able to predicate the ultimate strength to a large extent and the equation, for the most part, is on the conservative side as well.

$$v_c = 0.017\lambda\phi_c\sqrt{\rho E}\left(\frac{1}{D}\right)^{1/4}\sqrt{f_c'} \quad (2)$$

SUMMARY AND CONCLUSIONS

Based on the numerical analysis results obtained in this research study and considering the previous parameters, the following main conclusions are drawn:

1. Increasing the reinforcement ratio from 0.5 to 3.5% increased the shear capacity of the beams by 220%. The increase in the shear capacity was more pronounced for the specimen with the highest reinforcement ratio. The use of more reinforcement distributed uniformly across the circular cross section reduces the loss of flexural stiffness after cracking, increasing the neutral-axis depth and allowing the formation of more closely spaced cracks.

2. The results showed that the steel reinforced concrete (RC) specimen had the higher post-cracking stiffness and lower strain and deflection compared to the fiber-reinforced polymer (FRP)-RC specimens due to the higher axial stiffness of the steel reinforcing bars than FRP bars.

3. The shear capacity of RC-circular specimens with $a/d \leq 2.0$ is significantly dependent on the arch action. In contrast, specimens with $a/d \geq 2.5$ are dominated by beam action and the effect of a/d was insignificant. The ultimate strength at the failure stage increased between 24 and 316% due to the increase in the span-depth ratio from 1 to 5.5.

4. The result of this study indicated that increasing the member's depth reduced the deflection, strain, and the ultimate strength. The decrease in the stresses was roughly 12% and 16% for increasing the beam's diameter from 300 mm to 400 mm and 500 mm, respectively.

5. The regression analysis showed that the concrete contribution V_C to the shear strength is best described as a formula that is inversely proportional to the member's depth, and directly proportional to the square root of the axial stiffness of the reinforcement.

AUTHOR BIOS

Ahmed H. Ali *is an Assistant Professor in the Department of Civil Engineering, Faculty of Engineering, Helwan University, Cairo, Egypt. He received his BSc and MSc from the Faculty of Engineering, Helwan Univer-*

sity, in 2002 and 2008, respectively, and his PhD from the University of Sherbrooke, Sherbrooke, QC, Canada, in 2016. His research interests include the use of fiber-reinforced polymers (FRPs) in reinforced concrete structures.

Ahmed Gouda *is an Assistant Professor in the Department of Civil Engineering, Faculty of Engineering, at Helwan University. He received his BSc and MSc from the Faculty of Engineering, Helwan University, in 2002 and 2008, respectively, and his PhD from the University of Manitoba, Winnipeg, MB, Canada, in 2015. His research interests include the use of FRPs in reinforced concrete structures.*

Hamdy M. Mohamed *is an Associate Professor in the Department of Civil Engineering, Faculty of Engineering, at Helwan University. He received his PhD from the University of Sherbrooke. His research interests include the use and field applications of FRPs in reinforced concrete structures.*

Hala Mamdouh Esmael *is an Associate Professor in the Department of Civil Engineering, Faculty of Engineering, at Helwan University. She received her BSc and MSc from the Faculty of Engineering, Helwan University. Her research interests include the use of steel and FRPs in reinforced concrete structures.*

NOTATION

D	=	total diameter of circular member, mm
E	=	modulus of elasticity of the reinforcing bars, MPa
f_c'	=	specified compressive strength of concrete, MPa
V_c	=	concrete shear strength, N
ϕ_c	=	resistance factor for concrete
λ	=	factor accounting for concrete density

REFERENCES

Ali, A. H.; Gouda, A.; Mohamed, H. M.; Rabie, M. H.; and Benmokrane, B., 2020, "Nonlinear Finite Elements Modeling and Experiments of FRP-Reinforced Concrete Piles under Shear Loads," *Structures Journal*, V. 28, pp. 106-119. doi: 10.1016/j.istruc.2020.08.047

Ali, A. H.; Mohamed, H. M.; and Benmokrane, B., 2016, "Strength and Behavior of Circular FRP-Reinforced Concrete Sections without Web Reinforcement in Shear," *Journal of Structural Engineering*, ASCE, V. 04016196, doi: 10.1061/(ASCE)ST.1943-541X.0001684

Ali, A. H.; Mohamed, H. M.; and Benmokrane, B., 2016a, "Shear Behavior of Circular Concrete Members Reinforced with GFRP Bars and Spirals at Shear Span-to-Depth Ratios between 1.5 and 3.0," *Journal of Composites for Construction*, ASCE, V. 04016055, No. 6, p. 04016055 doi: 10.1061/(ASCE)CC.1943-5614.0000707

Ali, A. H.; Mohamed, H. M.; and Benmokrane, B., 2016b, "Strength and Behavior of Circular FRP-Reinforced Concrete Sections without Web Reinforcement in Shear," *Journal of Structural Engineering*, ASCE, V. 04016196, doi: 10.1061/(ASCE)ST.1943-541X.0001684

Ali, A. H.; Mohamed, H. M.; and Benmokrane, B., 2017, "Shear Strength of Circular Concrete Beams Reinforced with Glass-FRP Bars and Spirals," *ACI Structural Journal*, V. 114, No. 1, Jan.-Feb., pp. 39-49.

Ali, A. H., Mohamed, H. M., Benmokrane, B., and ElSafty, A., 2019, "Theory-Based Approaches and Microstructural Analysis to Evaluate the Service Life-Retention of Stressed Carbon Fiber Composite Strands for Concrete Bridge Applications." *Composites Part B: Engineering*, V. 165, pp. 279-292.

Ali, A. H.; Mohamed, H. M.; Chaallal, O.; Benmokrane, B.; and Ghrib, F., 2018, "Shear Resistance of RC Circular Members with FRP Discrete Hoops versus Spirals," *Engineering Structures Journal*, V. 174, pp. 688-700. doi: 10.1016/j.engstruct.2018.07.060

ACI Committee 440, 2015, "Guide for the Design and Construction of Concrete Reinforced with FRP Bars (ACI 440.1R-15)," American Concrete Institute, Farmington Hills, MI, 88 pp.

Andreaus, U.; dell'Isola, F.; Giorgio, I.; Placidi, L.; Lekszycki, T.; and Rizzi, N. L., 2016, "Numerical Simulations of Classical Problems in Two-Dimensional (Non) Linear Second Gradient Elasticity," *International Journal of Engineering Science*, V. 108, pp. 34-50. doi: 10.1016/j.ijengsci.2016.08.003

Bentz, E. C., 2000, "Sectional Analysis of Reinforced Concrete Members," PhD thesis, Department of Civil Engineering, University of Toronto, Toronto, ON, Canada, 184 pp.

Canadian Standards Association (CSA), 2012, "Design and Construction of Building Components with Fiber Reinforced Polymers (CAN/CSA S806-12)," CSA Group, Toronto, ON, Canada.

Canadian Standards Association (CSA), 2014, "Canadian Highway Bridge Design Code (CAN/CSA-S6-014)," CSA Group, Toronto, ON, Canada.

Canadian Standards Association (CSA), 2014, "Design of Concrete Structures (CAN/CSA A23.3-04)," CSA Group, Toronto, ON, Canada.

Cervenka, V.; Jendele, L.; and Cervenka, J., 2013, "ATENA Program Documentation Part 1: Theory," Cervenka Consulting Ltd., Prague, Czech Republic.

Cervenka, V.; Jendele, L.; and Cervenka, J., 2013, "ATENA Program Documentation Part 1: Theory," Cervenka Consulting Ltd., Prague, Czech Republic.

De Domenico, D.; Pisano, A. A.; and Fuschi, P., 2014, "An FE-Based Limit Analysis Approach for Concrete Elements Reinforced with FRP Bars," *Composite Structures*, V. 107, pp. 594-603. doi: 10.1016/j.compstruct.2013.08.039

El-Sayed, A. K.; El-Salakawy, E. F.; and Benmokrane, B., 2006, "Shear Strength of FRP-Reinforced Concrete Beams without Transverse Reinforcement," *ACI Structural Journal*, V. 103, No. 2, Mar.-Apr., pp. 235-243.

El-Sayed, A. K.; El-Salakawy, E. F.; and Benmokrane, B., 2006, "Shear Strength of FRP-Reinforced Concrete Beams without Transverse Reinforcement," *ACI Structural Journal*, V. 103, No. 2, Mar.-Apr., pp. 235-243.

Falope, F. O.; Lanzoni, L.; and Tarantino, A. M., 2019, "The Bending of Fully Nonlinear Beams. Theoretical, Numerical and Experimental Analyses," *International Journal of Engineering Science*, V. 145, p. 103167 doi: 10.1016/j.ijengsci.2019.103167

Halahla, A., 2018, "Study the Behavior of Reinforced Concrete Beam Using Finite Element Analysis," *Proceedings of the 3rd World Congress on Civil, Structural, and Environmental Engineering (CSEE'18)*, Paper No. ICSENM 103, Budapest, Hungary, Apr. 8-10, 2018. doi: 10.11159/icsenm18.103.10.11159/icsenm18.103

Halahla, A., 2018, "Study the Behavior of Reinforced Concrete Beam Using Finite Element Analysis," *Proceedings of the 3rd World Congress on Civil, Structural, and Environmental Engineering (CSEE'18)*, Paper No. ICSENM 103, Budapest, Hungary, Apr. 8-10, 2018. doi: 10.11159/icsenm18.103.10.11159/icsenm18.103

Hordijk, D. A., 1991, "Local Approach to Fatigue of Concrete," PhD thesis, Delft University of Technology, Delft, the Netherlands.

Jang, H. S.; Kim, M. S.; Cho, J. M.; and Kim, C. H., 2009, "Concrete Shear Strength of Beams Reinforced with FRP Bars According to Flexural Reinforcement Ratio and Shear Span to Depth Ratio," FRPRCS-9, Sydney, Australia.

Japan Society of Civil Engineers (JSCE), 1997, "Recommendation for Design and Construction of Concrete Structures Using Continuous Fiber Reinforcing Materials," Tokyo, Japan.

Kalpana, V. G., and Subramanian, K., 2011, "Behavior of Concrete Beams Reinforced with GFRP Bars," *Journal of Reinforced Plastics and Composites*, V. 30, No. 23, pp. 1915-1922. doi: 10.1177/0731684411431119

Lee, H.; Lee, H. S.; and Suraneni, P., 2020, "Evaluation of Carbonation Progress Using AIJ Model, FEM Analysis, and Machine Learning Algorithms," *Construction and Building Materials*, V. 259, p. 119703 doi: 10.1016/j.conbuildmat.2020.119703

Magliulo, G.; Ercolino, M.; Cimmino, M.; Capozzi, V. M.; and Manfredi, G., 2014, "FEM Analysis of the Strength of RC Beam-to-Column Dowel Connections under Monotonic Actions," *Construction and Building Materials*, V. 69, pp. 271-284. doi: 10.1016/j.conbuildmat.2014.07.036

Mohamed, H.; Ali, A. H.; and Benmokrane, B., 2016, "Behavior of Circular Concrete Members Reinforced with Carbon-FRP Bars and Spirals under Shear," *Journal of Composites for Construction*, ASCE, V. 04016090, doi: 10.1061/(ASCE)CC.1943-5614.0000746

Mohamed, H. M.; Ali, A. H.; and Benmokrane, B., 2019, "Mechanism of Distributed Composite GFRP Bars in Circular Concrete Members with and without Spirals under Shear," *Composites Part B: Engineering*, V. 162, pp. 62-72.

Mukhopadhyay, T.; Naskar, S.; Karsh, P. K.; Dey, S.; and You, Z., 2018, "Effect of Delamination on the Stochastic Natural Frequencies of Composite Laminates," *Composites Part B: Engineering*, V. 154, Dec., pp. 242-256. doi: 10.1016/j.compositesb.2018.07.029

Razaqpur, A. G., and Isgor, O. B., 2006, "Proposed Shear Design Method for FRP-Reinforced Concrete Members without Stirrups," *ACI Structural Journal*, V. 103, No. 6, Nov.-Dec., pp. 93-102.

Tureyen, A. K., and Frosch, R. J., 2002, "Shear Tests of FRP-Reinforced Concrete Beams without Stirrups," *ACI Structural Journal*, V. 99, No. 4, July-Aug., pp. 427-434.

Wang, Q.; Zhu, H.; Zhang, B.; Tong, Y.; Teng, F.; Su, W., 2020, "Anchorage Systems for Reinforced Concrete Structures Strengthened with Fiber-Reinforced Polymer Composites: State-of-the-Art Review," *Journal of Reinforced Plastics and Composites*, V. 39, No. 9-10, pp. 327-344.

ARE YOU A RESEARCHER?

SIGN UP FOR ORCID TODAY!

ORCID provides a persistent digital identifer that distinguishes you from every other researcher and, through integration in key research workflows such as manuscript and grant submission, supports automated linkages between you and your professional activities, ensuring that your work is recognized.

Individuals may use ORCID services freely and it's as easy as **1-2-3**:

1. REGISTER
2. ADD YOUR INFO
3. USE YOUR ORCID ID

For more information and to register, visit:

WWW.ORCID.ORG